



HAL
open science

Comanipulation Robotic Platform for Spine Surgery with Exteroceptive Visual Coupling: Development and Experimentation

Alizée Koszulinski, Juan Sandoval, Tanguy Vendeuvre, Saïd Zeghloul, Med Amine Laribi

► To cite this version:

Alizée Koszulinski, Juan Sandoval, Tanguy Vendeuvre, Saïd Zeghloul, Med Amine Laribi. Comanipulation Robotic Platform for Spine Surgery with Exteroceptive Visual Coupling: Development and Experimentation. *Journal of Medical Devices*, 2022, 16 (4), pp.041002. 10.1115/1.4054550 . hal-03668039

HAL Id: hal-03668039

<https://hal.science/hal-03668039>

Submitted on 14 May 2022

HAL is a multi-disciplinary open access archive for the deposit and dissemination of scientific research documents, whether they are published or not. The documents may come from teaching and research institutions in France or abroad, or from public or private research centers.

L'archive ouverte pluridisciplinaire **HAL**, est destinée au dépôt et à la diffusion de documents scientifiques de niveau recherche, publiés ou non, émanant des établissements d'enseignement et de recherche français ou étrangers, des laboratoires publics ou privés.

Comanipulation Robotic Platform for Spine Surgery with Exteroceptive Visual Coupling: Development and Experimentation

Alizée Koszulinski¹

Dept. GMSC - Pprime Institute,
CNRS - University of Poitiers - ENSMA, Poitiers, France
e-mail: alizee.koszulinski@univ-poitiers.fr

Juan Sandoval

Dept. GMSC - Pprime Institute,
CNRS - University of Poitiers - ENSMA, Poitiers, France
e-mail: juan.sandoval@univ-poitiers.fr

Tanguy Vendevre

CHU de Poitiers,
Dept. GMSC - Pprime Institute,
CNRS - University of Poitiers - ENSMA, Poitiers, France
e-mail: t.vendevre@gmail.com

Saïd Zegloul

Dept. GMSC - Pprime Institute,
CNRS - University of Poitiers - ENSMA, Poitiers, France
e-mail: said.zegloul@univ-poitiers.fr

Med Amine Laribi

Dept. GMSC - Pprime Institute,
CNRS - University of Poitiers - ENSMA, Poitiers, France
e-mail: med.amine.laribi@univ-poitiers.fr
ASME Member

ABSTRACT

¹ Corresponding author.

In this paper, a novel surgical robotic platform intended to assist surgeons in cervical spine surgery is presented. The purpose of this surgery is to treat the cervical spine instabilities. The surgical procedure requires drilling into specific region of the vertebrae in order to attach spinal implants and thus ensure a normal spacing between each vertebra concerned. In this context, the proposed robotic platform allows to control and restrict the surgeon's movements to a specific drilling direction set by the surgeon. The current platform is composed of a collaborative robot with 7 degrees of freedom (DoF) equipped with a drilling tool and directly comanipulated by the surgeon. A motion capture system, as an exteroceptive sensor device, provides the robot controller with the movement data of the vertebra to be drilled. Robot Operating System (ROS) framework is used to enable real-time communication between the collaborative robot and the visual exteroceptive device. In addition, an implemented compliance control program allows to enhance the safety aspect of the robotic platform. Indeed, the collaborative robot follow the patient's movements while constraining the tool movements to an optimal trajectory as well as a limited drilling depth selected by the surgeon. The collaborative robot's elbow movements are also restricted by exploiting the null-space in order to avoid collisions with other equipment or the medical team members. Experimental drilling trials have been performed by an orthopedic surgeon to validate the usefulness and different functionalities of the developed robotic platform, and provide that a collaborative robot can comply with a spine surgery procedure. These preliminary tests were performed in a lumbar spine model for which the use of a robotic device is most frequent due to a lower complexity compared to the cervical spine.

Keywords: *orthopedic surgical robot, spine surgery, drillings for pedicle screw placement, safety, exteroceptive visual coupling*

1 INTRODUCTION

1.1 Spine Surgery and Pedicle Screw Placements

Arthrodesis is a surgical technique that allows the fusion, i.e. the definitive consolidation, of at least two vertebrae. This operation allows the release of nerves and/or spinal cord, where these were previously compressed, as well as the stabilization

of the spine with the aim of maintaining a normal spacing between each vertebra concerned [1]. In order to do this, the surgeon has to drill holes in the vertebrae so that spinal implants can be fixed. These implants usually consist of pedicle screws, rods and plates.

The insertion of a cervical pedicle screw requires a thorough anatomical knowledge of each patient's vertebra to be drilled in order to know the optimal trajectory defined by an entry point, a direction, a diameter and a depth for each required hole. During an operation, the positioning of the drilling tool, according to this optimal trajectory corresponds to the pedicle aiming [2].

It is essential for the surgeon to be very accurate in order to preserve all the structures located around and inside the cervical spine. Indeed, a screw positioned too far medial to the vertebra could end up in the spinal canal and damage the spinal cord. Similarly, a screw that is too long or protrudes from the vertebral body could damage surrounding organs, vessels or tissues.

As robots for assisting orthopedic surgery are most frequently used at the lumbar spine level [3-4], a lumbar spine model has been used in the first development phase of the platform proposed in this paper. Indeed, compared to the thoracic spine and even more so to the cervical spine, the implantation of pedicle screws is easier at this level because of the larger size of the vertebrae and a lower mobility of the spine, mainly due to breathing. Nevertheless, compared to pedicle screw insertion in cervical spine, the pedicle aiming gesture, illustrated in Fig. 1., remains unchanged. The major differences

are the need for a larger diameter and greater depth of drilling in order to reach the vertebral body due to the larger size of lumbar vertebrae compared to the cervical ones.

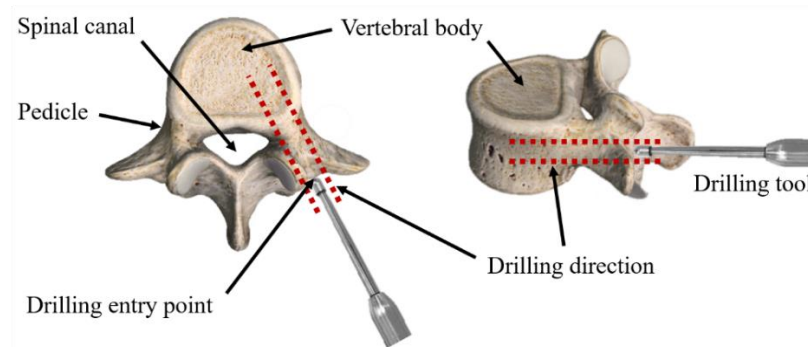


Fig. 1 Illustration of pedicle aiming for a lumbar vertebra

1.2 Contributions of Robotics

The integration of a robotic system for cervical surgery could increase the precision of the surgical gesture and thus allow finer drillings conferring a better stability of the screws. Indeed, the literature reports 8.3 to 50.3% of pedicle screws misplaced during the placement of spinal implants in conventional freehand surgery [5]. The possibility of using navigation systems has already considerably reduced these positioning errors in orthopedic surgery. For example, the article by Gelalis *et al.* [6] reporting the results of 26 studies with 6,617 screw positioning shows a percentage of perfectly positioned screws in the vertebral pedicle of 89-100% for navigation-assisted surgery. More recent studies, such as those reported by Molliqaj *et al.* [7], demonstrate the increase of accuracy with the use of comanipulation robotic devices, particularly for pedicle screw positioning in the thoracic spine. These results show the potential of using robotic systems considering the smaller size of the thoracic vertebrae pedicles compared to the lumbar vertebrae and therefore the increased accuracy offered by robotic devices.

In addition to the benefit in terms of accuracy, the use of a robotic device provides multiple advantages such as a reduction in the number of reoperations, infection rates, operating time and recovery time for patients [8].

1.3 Existing Robotic Devices for Orthopedic Surgery

Existing robotic devices can be classified into three categories: autonomous robots that completely replace the surgeon to perform the surgical gesture, teleoperation robots remotely controlled by the surgeon through a master interface and comanipulation robots being directly manipulated by the surgeon.

For autonomous robots, the planning of each gesture is needed as well as a recalibration between the virtual planning and the intraoperative situation so that the intervention is well carried out by the robot in the desired zone. The TSolution One [9] developed by THINK Surgical is fully automated to prepare bone cavities and joint surfaces of the hip and knee for implant placement. The surgical milling procedure is performed with the bone structures attached to the robotic platform by means of reference pins to ensure that these structures are fixed during the operation. Monogram's navigated surgical robot from Monogram Orthopedics [10], based on a KUKA iiwa robot and currently awaiting certification, has also been developed for hip and knee replacements but with a different philosophy. This robotic arm is combined with a marker tracking system, positioned on specific areas of the patient, in order to detect any movement of the patient and to adapt the robot trajectory in real time. In both cases, since the robot performs the milling procedure autonomously, the surgeon is kept completely out of the control loop regarding the realization of the surgical gesture.

To date, no robot for orthopedic surgery has been developed in a teleoperation mode. However, for illustration, we can mention the Da Vinci robot [11], marketed by the American company Intuitive Surgical, used for minimally invasive laparoscopic surgery. This platform is composed of two main elements: a manipulator (slave site) located close to the patient and made up of 4 robotic arms housing endoscopic instruments and a camera, and a remote haptic interface (master site) with which the surgeon remotely controls the instruments while visualizing their actions on the patient's anatomy.

Comanipulation robots are currently the most widespread robotic devices in the field of orthopedic surgery [12]: two strategies of use can be identified. The first one is to use the robot's end effector as a guide, like ROSA Spine [13] developed by Medtech, Mazor X Stealth [14] from Medtronic or the ExcelsiusGPS [15] produced by Globus Medical. These robots are used in particular to assist surgeons during drilling operations on the lumbar and thoracic spine. First, the robot positions itself autonomously along the drilling axis defined by the surgeon during the preoperative planning. The surgeon then slides the tool inside the guide. As the Monogram, these robotic systems are combined with a motion capture system to record the patient's movements, due to both breathing and the actions of the surgeon performing the procedure, and adapt their pose accordingly. The advantage of these systems is that they give the surgeon full tactile feedback when inserting the drilling tool into the bone, however, they also have some disadvantages. First of all, indeed for these devices to be usable in the operating room, it is necessary to plan each drilling procedure over a longer or shorter period of time in order to record the trajectories in the robot control. Furthermore, as the tool is not fixed

to the robot end effector, it is necessary to keep a cluster of markers on the tool, i.e. a set of markers representing a rigid body (see Fig. 2 (a)), which can therefore cause discomfort for the surgeon in terms of gripping the tool. Indeed, without this cluster it is impossible to recover the position of the tool tip and therefore to visualize its drilling progress in relation to the patient's anatomy.

A second strategy of comanipulation is to allow surgeon to directly manipulate the robotic arm. With the surgical tool attached to the end-effector of the robotic arm, it is possible to retrieve the position and orientation of the tool by the robot state data, thus eliminating the need for a marker cluster at the tool. Examples in this category are the VELYS robot [16] from DePuySynthes, a Johnson & Johnson company, and the MAKO [17] developed by Stryker mainly used in knee and hip surgeries.

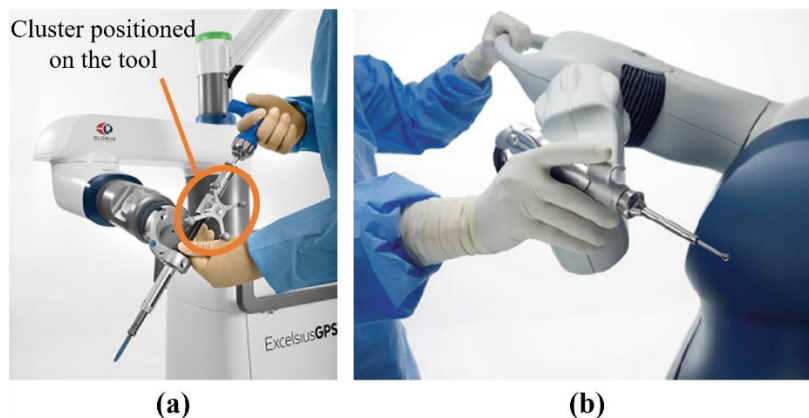


Fig. 2 Comanipulation robots ExcelsiusGPS (a) from Globus Medical and MAKO (b) developed by Stryker

1.4 Novel Robotic Device for Orthopedic Spine Surgery

Considering the abovementioned advantages, the last direct comanipulation strategy was chosen for the development of the new robotic platform presented in this paper. Indeed, this control mode is centered on the concept of keeping the control of the

robot by the surgeons, taking advantage of their dexterity and experience and combining it with the accuracy of a robotic device. Moreover, it allows to propose to the surgeons a new use of a robotic device for spine surgery, compared to the ROSA Spine or the ExcelsiusGPS, with an active motion of the robotic arm during the drillings which then assists and controls the whole gesture of the surgeon. A torque-control strategy, based on a compliance law, allows to generate a compliant behavior both in the working space and in the null-space. In addition to using only the internal sensors of the Franka Emika 7 DoF robot, the main advantage of this approach is that the robot is able to react to external forces applied on its overall body. Moreover, the motion of the robot's elbow, representing its degree of redundancy, is limited into a desired range thanks to a null-space compliance law in order to avoid any risk of collision with the equipment or medical staff located near the robot. A haptic depth motion restriction is also provided in the robot control by modifying the stiffness of the robotic arm according to the advance of the tool along the drilling axis. Furthermore, the tracking of the vertebra's movement combined with virtual guidance allowing the tool to remain in alignment with the desired drilling trajectory is an asset for learning the surgical procedure. An ergonomic tool holder adapted to the task has also been designed and allows in particular to consider the requirements in terms of space in an operating room thanks to its adaptability.

The key contributions of this work can be summarized as:

- 1) Development of a new robotic platform for spine surgery based on an active motion of a cobot, i.e. Franka Emika;

- 2) Fully compliance control strategy allowing the integration of virtual walls in order to constraint the drilling tool movements and exploiting the robot null-space to restrict the elbow's robot motion into a desired range inside an operating room;
- 3) Preliminary experimental validation of the robotic platform by an experimented orthopedic surgeon performing robot-assisted drilling tasks;
- 4) Development of a control mode suitable to assist novel surgeons in learning drilling gestures with optimal training as well as the performance evaluation during training.

This paper is then structured as follows: Section 2 describes the different elements of the robotic platform. Section 3 details the different control modes of the cobot and its functionalities. Section 4 presents and discusses the preliminary results. The last section concludes this paper.

2 THE ROBOTIC COMANIPULATION PLATFORM

2.1 Experimental Setup

The developed robotic platform is composed of Franka Emika Panda cobot, a collaborative robot with 7 DoF, to which the motorized surgical tool is attached at the flange by means of a holding fixture. The second main element of the platform is a motion capture system consisting of an Optitrack V120: Trio camera column, i.e. an exteroceptive visual device, and marker clusters. Figure 3 shows the proposed platform.

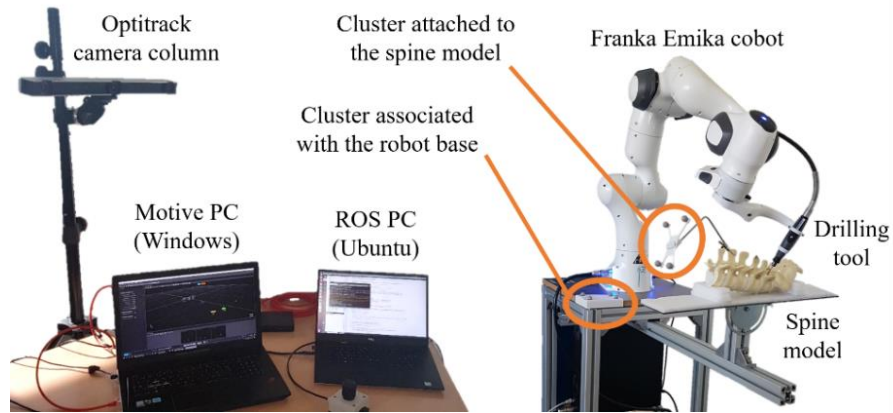


Fig. 3 Visualization of the different elements of the robotic platform

Two marker clusters are used: the first one, placed near to the robot base, allows the cameras to locate the robot in space whereas the second one, attached to a spine model, allows the motion tracking of the vertebra to be drilled. The spine model is fixed to the support of the robotic arm for practical reasons. During a real surgery, the robot will be totally independent from the operating table and thus from the patient. Nevertheless, these differences from the real scenario in an operating room have no impact on the working of the platform thanks to the use of marker clusters.

The operation of the robotic platform also requires the use of two separate computers communicating through a local network. The Motive PC, under Windows 10, is connected to the auto-calibrated Optitrack camera through the Motive software which streams the 6-DoF motion data of each cluster with a latency of less than 9 milliseconds, a positional accuracy of ± 0.2 mm and a rotational accuracy of ± 0.1 ° according to the manufacturer's instructions. It employs a NatNet networking protocol for the real-time transmission of the data of position and orientation of the marker clusters to the ROS PC. The latter, controlling the robot under the Robot Operating System (ROS) environment in Ubuntu 16.04 with PREEMPT-RT, allows the adaptation of the position and orientation of

the tool attached to the robot, according to the relative movements of the vertebra. This program thus allows the synchronization between the cobot and the Optitrack exteroceptive visual device.

In order to simulate a realistic environment for the surgeon as well as the tool manipulation during an operation, the coupling of the different elements of the platform required the design of a fixation support for the drilling tool, as detailed below.

2.2 Design of an Ergonomic Tool Holder

For the design of the tool holder, the latest evolution of surgical orthopedic tools, namely the surgical motors, has been considered. In fact, as mentioned in Section 1.3, this tool choice allows the tool to be fixed to the robotic arm and therefore does not require additional cluster tracking compared to the existing robotic devices for spine surgery which, to our knowledge, have been developed for the use of non-motorized tools such as pedicle probes and pedicle taps. As a result, the absence of a marker cluster at the level of the tool simplifies the procedure for surgeons who no longer have to worry about whether the tool cluster is constantly oriented towards the cameras and therefore perfectly detectable. The possibility to fix the motorized tool to the robotic arm also allows to know in real time the position and orientation of the tool thanks to the robot state's data provided by the robot's controller. It is thus possible to integrate arm virtual walls within the control program of the robotic in order to constrain in particular the drilling depth which is a critical parameter.

A first prototype of an ergonomic tool support was thus designed. This support corresponds to the assembly of six 3D printed parts: a base allowing the support to be

fixed to the flange of the robotic arm, a handle divided into 3 parts, a "cylindrical" holding piece allowing the drilling tool to be accommodated and a clamping part ensuring the tool is held inside the cylindrical piece.

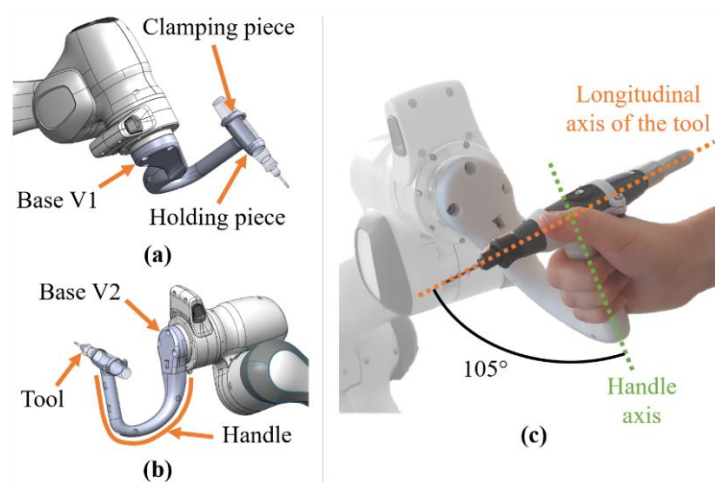


Fig. 4 (a)-(b) CAD models of the two configurations of the tool holder prototype and (c) visualization of the hand position on the real tool holder

The base of the tool holder was designed in two different versions allowing the tool to be held parallel (Fig. 4 - (a)) or perpendicular (Fig. 4 - (b)) to the last joint axis of the robotic arm. This design allows to take into account both, the space requirements in an operating room requiring for example a different configuration of the robotic arm (horizontal or vertical) and the surgeon's preferences. The handle allows the tool to be offset from the end of the robotic arm so that the surgeon's field of vision is not obstructed during the drilling process. In addition, it was designed considering the ergonomics of hand tools [18] in terms of inclination, diameter and handle length. Thus, this part allows a certain tilt between the handle and the tool, as shown in Fig. 4 – (c), in order to limit the stress on the wrist and thus guarantee the surgeon's comfort.

Since the robotic device requires a complete knowledge of its dynamic model in order to ensure optimal performance in terms of accuracy, stability and safety throughout the surgical procedure, the inertial parameters of the tool holder plus the drilling tool attached to the end-effector of the robot must be known and integrated into the robot controller. For this purpose, an identification procedure, proposed by [19] and based on least-squares estimation, was exploited comparing the joint torques provided by the robot to execute the same trajectory for two different conditions: with and without the tool attached to the robotic arm. This method has previously been validated on Franka Emika robots by Salah *et al.* [20].

3 ROBOTIC ARM CONTROL STRATEGY

In applications where the human is in the robot's workspace during the execution of a task, such as in the case of comanipulation robots, it is essential to ensure the safety of this user. Therefore, a torque-based impedance control strategy was implemented. In fact, this type of control strategy offers a compliant behavior, more precisely a spring-damper behavior, allowing to reduce the contact forces, i.e. the interaction forces between the robot and its environment [21-22]. In the context of surgical application, this can for example be used to reduce the risk of injury in case of collision between the robot and the surgeon or between the robot and the patient. The control law used is as follows:

$$\boldsymbol{\tau}_c = \boldsymbol{\tau}_{\text{task}} + \boldsymbol{\tau}_{\text{null}} + \boldsymbol{\tau}_{\text{comp}} \quad (1)$$

where $\boldsymbol{\tau}_c$ is the vector of control torques, $\boldsymbol{\tau}_{\text{task}}$ is associated with the task, $\boldsymbol{\tau}_{\text{null}}$ allows the exploitation of the robot's degree of redundancy and $\boldsymbol{\tau}_{\text{comp}}$ is the vector of torques corresponding to the gravitational compensation of its own weight.

The robot's trajectory is therefore controlled using the vector $\boldsymbol{\tau}_{\text{task}}$. The latter is calculated from the desired Cartesian trajectory, noted \mathbf{X}_d , such as:

$$\boldsymbol{\tau}_{\text{task}} = \mathbf{J}^t \cdot \mathbf{F}_{\text{task}} = \mathbf{J}^t \cdot [\mathbf{K}_p \cdot (\mathbf{X}_d - \mathbf{X}) - \mathbf{K}_d \cdot \dot{\mathbf{X}}] \quad (2)$$

where \mathbf{F}_{task} is the vector of external forces on the 6 DoF of the Cartesian space. \mathbf{K}_p and \mathbf{K}_d are diagonal matrices associated with the stiffness and damping values, respectively, allowing to adjust the compliant behavior of the robot. \mathbf{J} is the Jacobian matrix, \mathbf{X} and $\dot{\mathbf{X}}$ correspond respectively to the current cartesian positions and velocities of the robot.

3.1 Control Modes of the Platform

By exploiting the impedance control law, different control modes have been implemented to define an initial scenario for using the platform.

3.1.1 Free Manual Guidance Mode

To begin, a free manual guidance mode was implemented. This mode allows the surgeon to freely hand-guide the robotic arm within the robot workspace. As abovementioned, in the spine surgery application, this mode allows the surgeon to locate the tool at the desired drilling entry point and in the desired direction. In this control mode, only the torque vector associated with the weight and friction compensation is kept in the control law, which then becomes:

$$\boldsymbol{\tau}_c = \boldsymbol{\tau}_{\text{comp}} \quad (3)$$

Thus, the forces exerted by the surgeon on the robotic arm modify the configuration of the latter, which at each moment compensates its own weight without opposing to the surgeon's movements.

3.1.2 Vertebra Motion Tracking and Drilling Mode

Once the tool is positioned according to the desired trajectory, i.e. at a specific entry point and according to the desired drilling direction, a vertebra-motion tracking mode can be activated. This second control mode allows on the one hand to follow the movements of the targeted vertebra but also to constrain the movements of the tool to its longitudinal axis only (see Fig. 4 – (c)) thus allowing to assist the drilling gesture.

The aim is to release the tool along the drilling axis so that the surgeon can control the forward of the tool inside the patient's vertebra. Out of this direction, a suitable stiff behavior is applied so that the chosen direction is fulfilled.

The desired position and orientation of the tool are determined in real-time through the transformation matrix calculations presented in Appendix. In parallel, the release of the tool along the drilling axis is possible by modifying the stiffness matrix \mathbf{K}_p of the robotic arm. The first three values of this diagonal matrix are related to the cartesian translational motion and the subsequent three values are associated with the cartesian rotational motion, yielding:

$$\mathbf{K}_p = \begin{bmatrix} K_{p_x} & 0 & 0 & 0 & 0 & 0 \\ 0 & K_{p_y} & 0 & 0 & 0 & 0 \\ 0 & 0 & K_{p_z} & 0 & 0 & 0 \\ 0 & 0 & 0 & K_{p_{rx}} & 0 & 0 \\ 0 & 0 & 0 & 0 & K_{p_{ry}} & 0 \\ 0 & 0 & 0 & 0 & 0 & K_{p_{rz}} \end{bmatrix} \quad (4)$$

Initially, the translational stiffness values are equal and set to 700 N/m while the rotational stiffness are set to 30 N/rad. These values correspond to the maximum stiffness values permissible by the Franka robot and provide a sufficient stiff behavior to the tool.

In our case, the opposite effect in terms of rigidity is sought along the longitudinal axis of the tool so that it can be freely moved along the desired drilling axis. In this sense, a zero stiffness must be applied along the \vec{z} axis of the tool. However, since the previously indicated stiffness values are associated with the axis of the robot base frame and not with those of the tool frame, the determination of a 6x6 transformation matrix was necessary. The method for computing this type of matrix is explained in [19] and was followed as:

$${}^T\mathbf{M}_F = \begin{pmatrix} 1 & 0 \\ \mathbf{S}({}^T\mathbf{P}_F) & 1 \end{pmatrix} \begin{pmatrix} {}^T\mathbf{R}_F & 0 \\ 0 & {}^T\mathbf{R}_F \end{pmatrix} = \begin{pmatrix} {}^T\mathbf{R}_F & 0 \\ \mathbf{S}({}^T\mathbf{P}_F){}^T\mathbf{R}_F & {}^T\mathbf{R}_F \end{pmatrix} \quad (5)$$

$$\text{where } \mathbf{S}(\mathbf{P}) = \begin{pmatrix} 0 & -P_z & P_y \\ P_z & 0 & -P_x \\ -P_y & P_x & 0 \end{pmatrix}$$

This new transformation matrix is then calculated at each time so that the drilling axis, according to which the stiffness of the robotic arm is zero, is constantly function of the movements of the vertebra. The vector of external forces thus becomes:

$$\mathbf{F}_{\text{task}} = {}^T\mathbf{M}_F^t \cdot \mathbf{F}_{\text{taskT}} \quad (6)$$

$$\text{where } \mathbf{F}_{\text{taskT}} = \mathbf{K}_{pT} \cdot \Delta\mathbf{X}_T - \mathbf{K}_{dT} \cdot \dot{\mathbf{X}}_T = \mathbf{K}_{pT} \cdot {}^T\mathbf{M}_F (\mathbf{X}_d - \mathbf{X}) - \mathbf{K}_{dT} \cdot {}^T\mathbf{M}_F \cdot \dot{\mathbf{X}}$$

Consequently, the implemented control mode allows an adjustable guidance level of the tool along the desired direction of motion. Indeed, very high stiffness values in the transverse directions of the motion axis would force the drill to only be moved along the desired motion axis, whereas lower stiffness values would tolerate deviations of the drill from the desired motion axis. Thus, a damped elastic behavior is generated around the desired motion axis, as illustrated in Fig. 5.

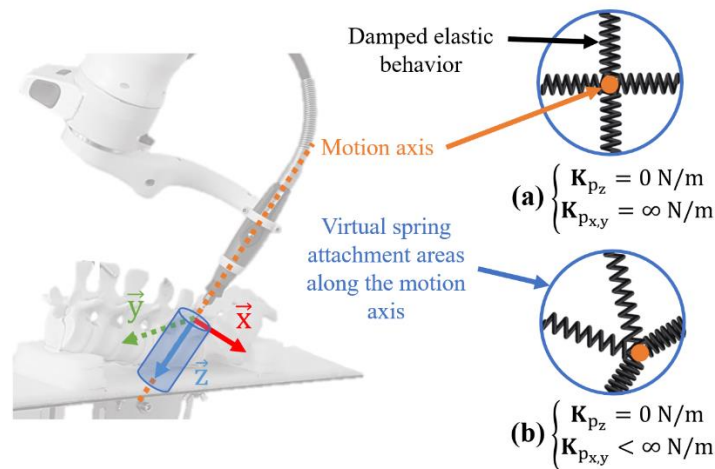


Fig. 5 Representation of the damped elastic behavior induced by the stiffness modification in the transverse directions of the motion axis. In the case of very high stiffness the drill is kept along the desired motion axis (a) while low stiffness values produce tolerated deviations of the drill from the desired motion axis (b)

This behavior can be more or less elastic depending on the stiffness imposed along the transverse directions. In fact, by varying the imposed stiffness, the opposition forces generated by the damped elastic behavior can be modified. In this way, we can regulate the degree of assistance during the drilling process. This concept can be used in particular in the context of surgical training programs.

Concerning the control mode switches, these can only be performed by an assistant following the surgeons' verbal instructions at the moment. Indeed, the robotic platform is currently equipped with a joystick which will be replaced by a foot pedal plate in order to be suitable for use in operating room and directly activated by surgeons. Furthermore, a change of control mode can be decided by the surgeon at any time. In this sense, the proposed platform is able to cope with many clinical scenarios. For example, if the surgeon wishes to correct the initially defined drilling trajectory, it is possible to change the control mode at any time in order to manually replace the drilling tool and to continue the drilling in progress by reactivating the vertebral motion tracking mode.

3.2 Safety Functionalities of the Platform

In addition to the displacement constraint applied to the tool in the vertebra motion tracking mode, other safety functionalities to assist the surgeon's gesture have been developed.

3.2.1 *Virtual Walls to Avoid the Risk of Collisions*

Taking advantage of the degree of redundancy of the Franka robot, virtual walls were implemented to restrict the robot elbow motion, based on [22] whose work focused on the KUKA LWR 4+ robot. These walls aim to avoid any risk of collisions with equipment close to the patient (e.g. O arm, instrument table), surgeons or other members of the medical team.

The Franka Emika robot is a 7 DoF anthropomorphic robot. Indeed, it has one additional DoF compared to those needed to perform a task in Cartesian space (requiring three for translation and three for rotation). This additional DoF can be represented by the tilt of the robot's elbow. This tilt is associated with an angle Ψ of the plan formed by the shoulder, elbow and wrist of the robot around the shoulder-wrist axis, as shown in Fig. 6. The angle Ψ can geometrically be determined from the joint positions \mathbf{q} of the robot. Two limits Ψ_{\min} and Ψ_{\max} , represented in Fig. 6, can be defined by manually positioning the robot in the desired limit configurations and recording the associated joint positions.

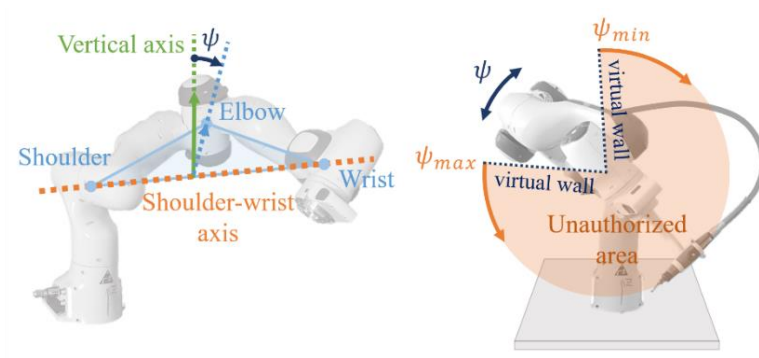


Fig. 6 Redundancy representation of the Franka Emika cobot. The desired virtual walls of the robot null-space are defined from the values of the limit angles ψ_{min} and ψ_{max} of the robot elbow.

Between these two limits, the robot's elbow is intended to freely move without causing any additional movement to the tool, preserving the drilling task. Beyond these limits, a force is applied by the robot in order to constrain the movement of the elbow and to keep the tilt of the latter within the desired range $[\psi_{min}, \psi_{max}]$.

To do this, the null-space torque vector is defined as follows outside the imposed limits:

$$\boldsymbol{\tau}_{null} = \begin{cases} \mathbf{N}(\mathbf{q}) \cdot [\mathbf{K}_{p\psi} \cdot (\mathbf{q}_{\psi_{min}} - \mathbf{q}) - \mathbf{K}_{d\psi} \cdot \dot{\mathbf{q}}] & \text{for } \psi \leq \psi_{min} \\ \mathbf{N}(\mathbf{q}) \cdot [\mathbf{K}_{p\psi} \cdot (\mathbf{q}_{\psi_{max}} - \mathbf{q}) - \mathbf{K}_{d\psi} \cdot \dot{\mathbf{q}}] & \text{for } \psi \geq \psi_{max} \end{cases} \quad (7)$$

where $\mathbf{N}(\mathbf{q}) = \mathbf{I} - \mathbf{J}^t \mathbf{J}^{+t}$ is the null-space projector, $\mathbf{K}_{p\psi}$ the null-space stiffness matrix,

$\mathbf{K}_{d\psi} = 2\sqrt{\mathbf{K}_{p\psi}}$ the damping matrix, $\mathbf{q}_{\psi_{min}}$ and $\mathbf{q}_{\psi_{max}}$ the joint coordinates associated with the desired minimum or maximum limit.

The possibility of integrating virtual walls improves the safety of the platform with respect to members of the medical team and equipment other than the robot by preventing the risk of collisions. With regard to patient safety, a virtual stop has been

defined in addition to the constraint of the tool's movements along its longitudinal axis, as explained in the next section.

3.2.2 *Virtual Safety Stop to Control the Drilling Depth*

A certain precision is also required in terms of drilling depth so that the drilling does not go beyond the vertebral body located on the anterior part of each vertebra. By implementing a virtual safety stop, we thus seek to preserve the organs, vessels or tissues around the vertebra to be drilled by controlling and restricting the surgeon's movement along the drilling axis (see Fig. 7). The idea is that the robot exerts a force opposite to the surgeons' movement, thus preventing them from drilling beyond the desired depth. Moreover, the application of this force must not be too brutal so that the surgeon does not feel an abrupt opposition and so that it does not generate any tremor in the tool. The aim is to reverse the release of the tool along the drilling axis by increasing the stiffness, then equal to zero, from a certain limit.

In order to ensure that the stiffness evolution does not depend on the tool feed speed, i.e. the drilling time, and stop the surgeon motion in a safe way. A stiffness evolution as a function of the tool tip position along the drilling axis has then been defined. We have therefore implemented a non-linear stiffness behavior similar to the viscoelastic behavior of the most compliant part of the human body, namely the abdomen, and whose model has recently been implemented in a compliant mechanism proposed by [23-24]. We then applied an attenuation coefficient so that the maximum stiffness reached is equal to 700 N/m as shown in Fig. 8.

Initial tests were carried out to evaluate the haptic feedback for the surgeon in terms of opposition effort. In addition, we checked that the increase in stiffness did not cause any tremor at the tool.

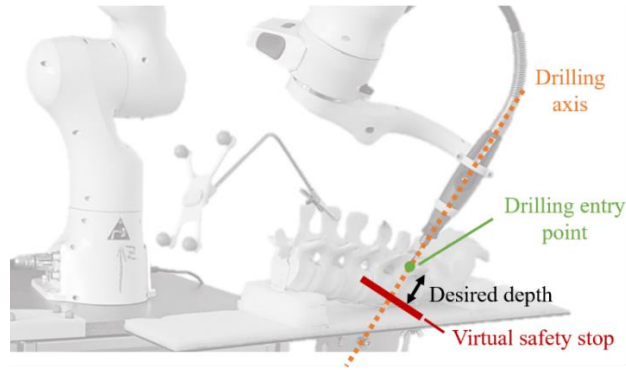


Fig. 7 Representation of the virtual safety stop in relation to the spine model and the tool position

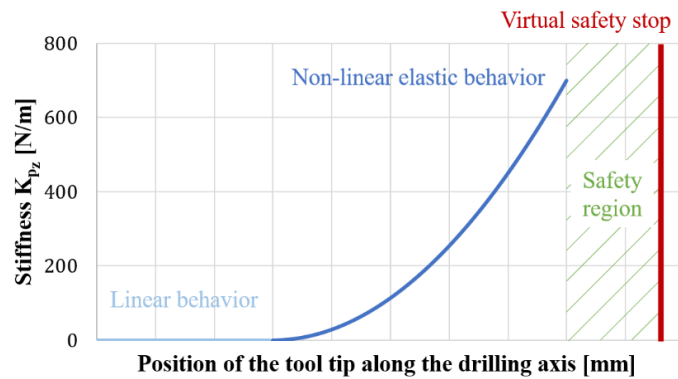


Fig. 8 Evolution of the robot stiffness along the longitudinal axis of the tool

The maximum stiffness of 700 N/m is reached upstream of the desired drilling depth to ensure that the limit is never reached by maintaining a safety region.

The proposed stiffness behavior thus allows surgeons to have the same sensations in terms of opposition force for each drilling. Indeed, the differences that the surgeon may feel between each drilling will be only due to the mechanical resistance of the patient's vertebrae.

4 PRELIMINARY EXPERIMENTS

4.1 Validation of Vertebra Motion Tracking

In order to evaluate the use of the robotic platform, its theoretical accuracy in terms of motion tracking was first determined. For this purpose, a random motion of the spine model was acquired. In addition to the marker clusters of the robot base and the spine model, represented in Fig. 3, a marker was placed on the spine model to symbolize a drilling entry point and thus obtain the real position of the entry point based on the movement of the spine model. As the spine is not a rigid segment due to the viscoelastic intervertebral discs, the lumbar model used, faithful to reality, has elastic parts reproducing the behavior of the discs. This internal mobility therefore leads to errors in terms of movement tracking if the cluster is not attached to the vertebra being drilled. Knowing this, the additional marker was attached to the same vertebra to which the spine cluster was fixed. In parallel, the theoretical position of the drilling entry point in relation to the robot base frame was computed from the initial position of the entry point and the use of the geometrical transformation presented in Appendix. Figure 9 shows the evolution of the real and calculated theoretical position of the drilling entry point during the random movement recorded for 5 seconds and corresponding to 600 frames. The relative errors were also calculated and the results for each directions of space are represented in the same figure.

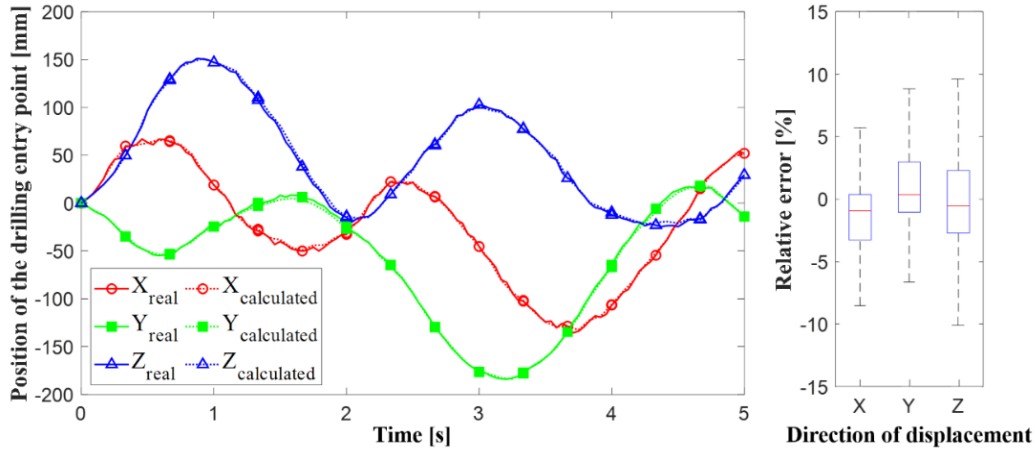


Fig. 9 Evolution of the real and calculated position of the drilling entry point as a function of time and position relative errors considering each directions of displacement

The results obtained show that the theoretical position of the drilling entry point, which corresponds to the instruction sent to the robot in the vertebra motion tracking control mode (see subsection 2.1.3), is correctly calculated. Indeed, the curves of expected and calculated position for each direction are overlapped and the relative errors are about $\pm 10\%$. Considering movements of the order of centimeters, induced for example by respiratory movements, the tracking errors are of the tenth order of a millimeter. These errors are due to the Optitrack system accuracy as well as to the calculation errors of the numerous geometrical transformations necessary to express the coordinates of the drilling entry point in the robot base frame according to the movements of the vertebra.

4.2 Effect of Robot Stiffness Settings on the Trajectory of the Tool

Secondly, a comparative evaluation on drilling performance, and more precisely on the ability to maintain a linear tool movement direction, with different stiffness settings has been conducted. An operator was thus asked to move the drilling tool, fixed

to the robotic arm, along its longitudinal axis while maintaining a trajectory as linear as possible over a distance of about 100 mm. This test was repeated three times, each time changing the stiffness values along the transverse axis of the tool, i.e. the x and y-axis, in the drilling control mode presented in subsection 3.1.2. Transverse stiffnesses $K_{p_{x,y}}$ equal to 0, 350 and 700 N.m/rad were thus applied, corresponding to degrees of assistance of 0, 50 and 100% respectively, in accordance with the maximum stiffness that can be imposed on the Franka Emika robot, i.e. 700 N.m/rad as mentioned previously in subsection 3.1.2. Moreover, in order to better visualize the performance evolution according to the degree of assistance provided by the platform, these tests were performed by an unexperienced operator and not by a skilled surgeon accustomed to the drilling procedure.

For each applied transverse stiffness value, the evolutions of the position of the tool tip along the x-and-y axis as a function of the longitudinal displacement of the tool have been computed in relation to the initial tool frame using the data provided by the robot's controller. The positions of the tool along the transversal axis having been calculated according to the initial tool frame, the evolution of the latter along the z-axis of the tool should be equal to zero, thus indicating that the desired trajectory has been fully respected. The results are shown in Fig. 10.

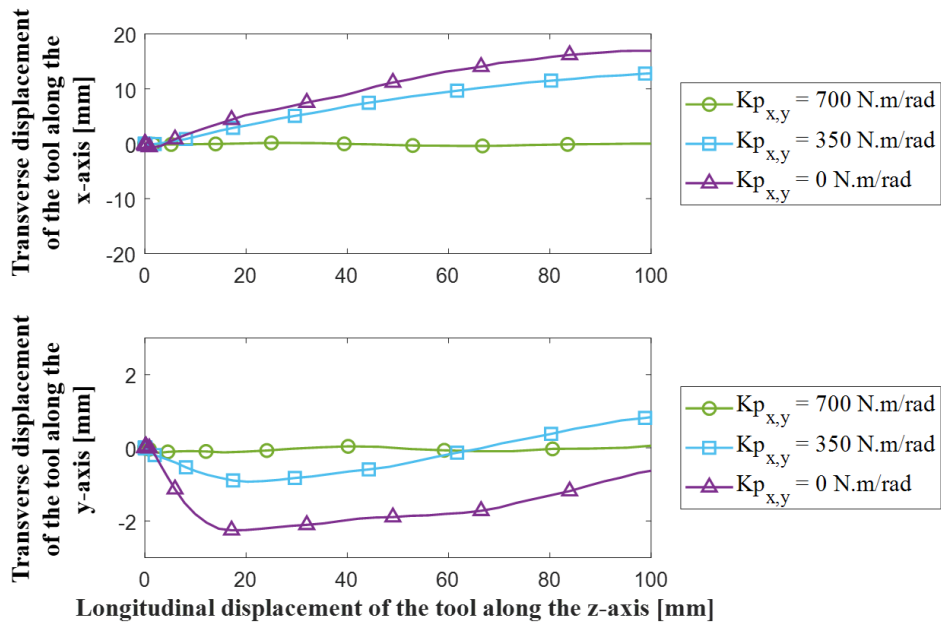


Fig. 10 Evolution of the position of the tool tip along the x-and-y axis as a function of the longitudinal displacement of the tool and the values of the applied transverse stiffnesses

First, the curves obtained from the evolution of the tool position show that the lower the transverse stiffnesses applied to the tool, i.e. the lower the degree of assistance of the platform, the greater the deflections of the tool. Indeed, the positioning deviations with a maximum degree of assistance are close to zero in both transverse directions while when the tool displacements are not constrained, i.e. with $K_{p_{x,y}}$ equal to 0 N.m/rad, deviations of more than 2 mm along the y-axis and almost 17 mm along the x-axis are observed. These results show the efficiency of the control mode implemented in order to guarantee the strict respect of the desired drilling trajectory.

These tests also show the possibility to follow the improvement of the surgeons' performances during the learning phase of the drilling gesture.

These tests also show the possibility to follow the improvement of surgeons' performance during the learning phase of the drilling gesture. In fact, surgeons will be able to visualize

the evolution of their performances as the drilling are made thanks to the processing of data transmitted in real time by the robot's controller.

4.3 Experimental Drilling Tests Assisted by the Robotic Platform

Subsequently, an evaluation of the repeatability and accuracy of drillings assisted by the proposed robotic platform was carry out. For these preliminary tests, an orthopedic surgeon was asked to perform a total of 6 drillings in the lumbar spine model. The different control modes of the robot were first explained to the surgeon so that he could be able to communicate to an assistant the desired control mode changes during the different phases of the test. In order to be able to evaluate only the accuracy of the drillings, particularly in terms of depth, and not the combined effect with the tracking of vertebrae movement, the spine model was fixed to its support. In addition, as explained in subsection 4.1, the spine model has elastic parts reproducing the viscoelastic behavior of the real intervertebral discs which leads to errors in terms of movement tracking if the cluster is not attached to the vertebra being drilled. In order to rigidify the lumbar spine model, the model have been fixed to its support, thus allowing the surgeon to perform drillings in several vertebrae without having to move the marker cluster. In a real surgery, i.e. with a mobile spine, this cluster will necessarily have to be as close as possible to the vertebra to be drilled, as is the case in conventional surgery involving the use of a optic navigation system composed of an imaging device (e.g. O-arm) and a motion capture system [25-26]. Moreover, as shown in Fig. 11, foam bases were also added on either side of the spine model to reproduce the lordosis, i.e. the natural curvature of the lumbar spine.

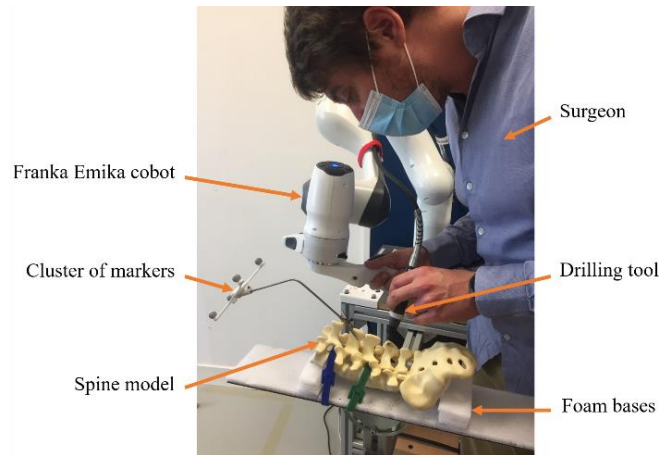


Fig. 11 Photo of an experimental drilling trial carried out by an orthopedic surgeon in the spine model in order to validate the first functionalities of the robotic platform

For these tests, a stiffness of 700 N.m.rad^{-1} was applied along the \vec{x} and \vec{y} axes of the tool and a virtual stop of 20 mm was chosen due to the constraint of the length of the drill (of about 25 mm) used for the experiments.

The evolution of the position and orientation of the drilling tool as well as the force measured at the tool were recorded from the data sent by the robot and are shown in Fig. 12. Concerning the force recorded, the robot is equipped with external force sensors at each of its joints. Thus, it is possible to compute the forces applied at the tool by using the Jacobian matrix. For instance, according to section 3.2.2., once the stiffness K_{pz} increases when approaching the virtual safety stop, the robot's motion along the z-axis is restricted to avoid exceeding the virtual safety stop. Therefore, any motion intended by the surgeon to exceed this limit will be measured by the robot as an external force. A similar behavior is encountered along the transversal x and y-axis.

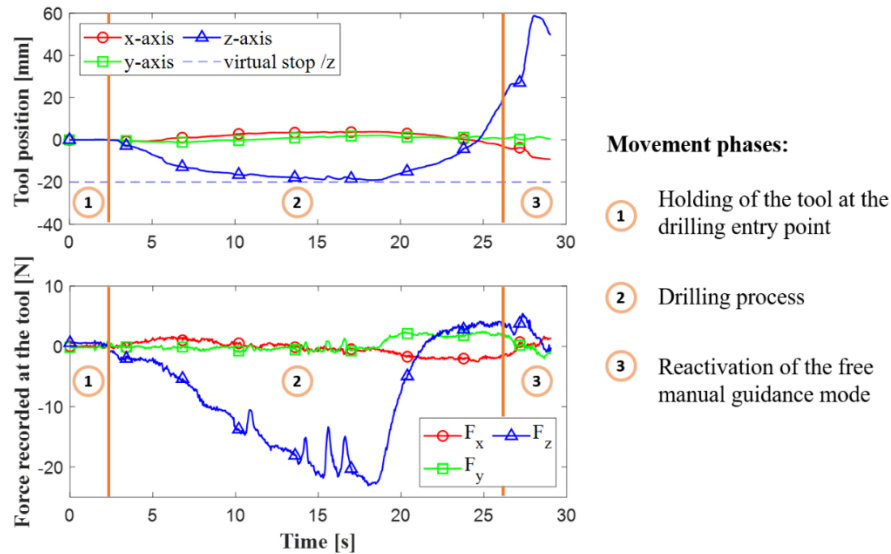


Fig. 12 Example of results obtained in terms of evolution of the position of the tool tip with respect to the initial tool reference frame $\{T\}$ and evolution of the force exerted on the tool

In Fig. 12, the first phase of the movement corresponds to the holding of the tool at the entry point of the drilling, the free positioning of the tool according to the desired trajectory having been carried out beforehand. The second phase is associated with the drilling gesture carried out following the activation of the vertebra-tracking and assisted-drilling mode. At the end of the surgical procedure, the free manual guidance mode is reactivated corresponding to the last movement phase observable on the curves.

As explained in Section 3.2.2, an opposition force is generated by the robot due to the increase of the robot stiffness along the drilling axis defined as a function of the tool depth in relation to the drilling entry point. Thus, during the first 3 seconds of drilling, a force close to zero is recorded, which means that the robot does not oppose the advancement of the tool which is far from the limit depth of drilling. Then, according to the surgeon's feedback, an increasing opposition force is felt until it is maximal at the level of the chosen virtual stop (here 20 mm). The surgeon's movement is thus blocked and the

drilling tool is then extracted from the concerned vertebra. In addition, peaks in force are observed in the middle of the drilling phase. These are due to small back and forth movements made as the virtual stop is approached, leading to a decrease in the perceived force and then a reincrease until a maximum opposition force of 23.1 N is reached. Thus, the evolution of the tool tip position along the \vec{z} axis, the longitudinal axis of the drilling tool, is tangent to the horizontal line representing the virtual safety stop (dotted blue line in Fig. 12).

Table 1 Results of the experimental drilling trials carried out on the spine model

Drilling tests	n°1	n°2	n°3	n°4	n°5	n°6
Maximum drilling depth [mm]	16.6	17.9	18.7	19.7	19.1	19.9
Maximum recorded force [N]	16.3	18.5	20.7	26.7	23.1	26.0

Table 1 shows the evolution of the drilling depths and the maximum force measured at the maximum of this depth over the six drillings performed by the surgeon. These results reveal that all the holes drilled are well below the virtual stop of 20 mm. However, only half of the holes appear to have been drilled to the desired virtual stop. Indeed, the first three holes have been drilled to a depth of less than 19 mm. The need for the surgeon to adapt to the use of the platform and the haptic feedback may explain this phenomenon. Indeed, the increase in the maximum force exerted on the tool as the holes are drilled may be synonymous with the appropriation of the robotic device by the surgeon.

5 CONCLUSION AND FUTURE WORK

In this paper, a new comanipulation robotic platform intended to assist surgeons for spine surgery has been presented. The proposed platform is composed of an exteroceptive visual system used to track the vertebra movements in real time and to modify the pose of a drilling tool, attached to the end of a robotic arm, accordingly. The main advantage of this platform compared to existing ones for spine surgery is the possibility for the surgeon to directly manipulate the robotic arm. This configuration makes it possible to eliminate the cluster that was previously placed on the tool, which could have hindered its manipulation during drilling. In fact, the progress of the tool in relation to the patient's anatomy can be known directly thanks to the data transmitted by the robot. Moreover, the developed robotic platform, entirely designed in a comanipulation scheme, fits into the surgical procedure currently followed by surgeons without involving major modifications. Indeed, the surgeon is required to perform the same gestures as in a conventional operation. The only notable difference is that the robot supports the tool at the same time as the surgeon and then constrains its movements to the desired drilling axis. The different control modes implemented thus allow surgeons to freely position the tool according to the desired optimal trajectory and then proceed with the drilling while following the patient's movements. Furthermore, a non-linear elastic behavior has been generated in the longitudinal axis of the tool, i.e. the drilling axis, in order to control the drilling depth to a predefined safety limit. In parallel, the robot's elbow movements can be limited to avoid any risk of collisions by exploiting the robot's null-space. Preliminary experimental results and feedback from an

experimented orthopedic surgeon validated the use of the robotic platform, particularly in terms of repeatability and accuracy for drilling depth.

Further tests are needed to quantify the surgical performance with and without robotic assistance for a moving spine model whose movements will then be tracked. Future work will therefore focus on conducting these additional and comparative experiments, taking into account outcomes related to the time required to perform the drilling tasks, the accuracy and the repeatability of their execution by experimented and unskilled surgeons.

ACKNOWLEDGMENT

This work was supported by the University of Poitiers and by the CNRS, the French National Centre for Scientific Research, through the International Research Project RACeS (Robotic Assisted System for Safe Cervical Surgery), TWN-IRP-17, <https://irp-races.prd.fr/>.

NOMENCLATURE

${}^F\mathbf{T}_V$	transformation matrix between the robot base frame $\{F\}$ and the reference frame $\{V\}$ of the cluster attached to the vertebra
${}^F\mathbf{T}_R$	transformation matrix between the robot base frame $\{F\}$ and the reference frame $\{R\}$ of the robot support
${}^R\mathbf{T}_V$	transformation matrix between the reference frame $\{R\}$ of the robot support and the reference frame $\{V\}$ of the cluster attached to the vertebra
\mathbf{I}	identity matrix
${}^F\mathbf{P}_R$	coordinates of the origin of the robot support reference frame $\{R\}$ in the robot base frame $\{F\}$
${}^C\mathbf{T}_R$	transformation matrix between the cameras reference frame $\{C\}$ and the reference frame $\{R\}$ of the robot support
${}^C\mathbf{T}_V$	transformation matrix between the cameras reference frame $\{C\}$ and the reference frame $\{V\}$ of the cluster attached to the vertebra
${}^{\text{virtual } V}\mathbf{T}_D$	transformation matrix between the virtual frame $\{\text{virtual } V\}$ located on the vertebra cluster and the drilling entry point frame $\{D\}$
${}^{\text{virtual } V}\mathbf{P}_D$	coordinates of the drilling entry point in the virtual frame $\{\text{virtual } V\}$ located on the vertebra cluster
${}^F\mathbf{T}_D$	transformation matrix between the robot base frame $\{F\}$ and the drilling entry point frame $\{D\}$

${}^F\mathbf{T}_{\text{virtual V}}$	transformation matrix between the robot base frame $\{F\}$ and the virtual frame $\{\text{virtual V}\}$ located on the vertebra cluster
$\boldsymbol{\tau}_c$	vector of control torques
$\boldsymbol{\tau}_{\text{task}}$	vector associated with the task
$\boldsymbol{\tau}_{\text{null}}$	vector allowing the exploitation of the robot's degree of redundancy
$\boldsymbol{\tau}_{\text{comp}}$	vector of torques corresponding to the gravitational compensation of its own weight
\mathbf{X}_d	desired Cartesian trajectory
\mathbf{J}	Jacobian matrix
\mathbf{F}_{task}	vector of external forces on the 6 DoF of the Cartesian space
\mathbf{K}_p	diagonal matrix associated with the stiffness values
\mathbf{K}_d	diagonal matrix associated with the damping values
\mathbf{X}	current cartesian positions of the robot
$\dot{\mathbf{X}}$	current cartesian velocities of the robot
${}^T\mathbf{M}_F$	6x6 transformation matrix between the tool reference frame $\{T\}$ and the robot base frame $\{F\}$
${}^T\mathbf{R}_F$	rotation matrix between the tool reference frame $\{T\}$ and the robot base frame $\{F\}$
ψ	angle of the plan formed by the shoulder, elbow and wrist of the robot around the shoulder-wrist axis

- \mathbf{q}** joint position of the robot
- $\mathbf{N}(\mathbf{q})$** null-space projector

APPENDIX. Geometrical Transformations

Five reference frames were defined as shown in Fig. 13: $\{C\}$ is the reference frame of the Optitrack cameras, $\{F\}$ is the frame of the Franka Emika's base, $\{R\}$ is the frame associated with the cluster placed on the robot's support, $\{T\}$ is related to the tool and $\{V\}$ is linked to the cluster attached to the vertebra.

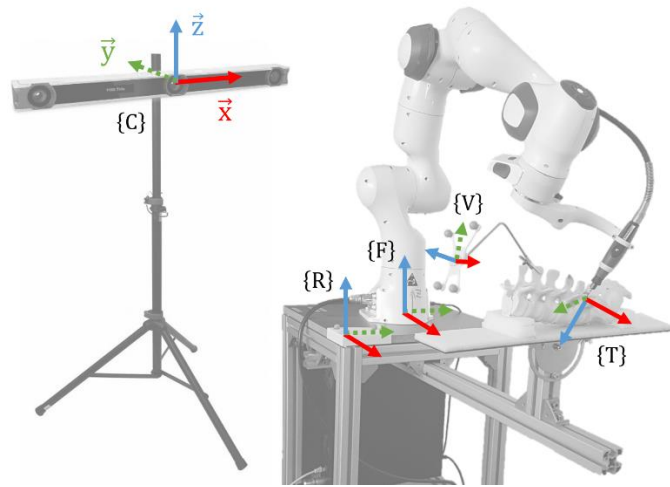


Fig. 13 Reference frames definition for each element of the robotic platform

The reference frame $\{R\}$, fixed with respect to the robot's base, allows the camera to locate the latter in space and therefore enhance the synchronization between the data coming from the camera and the robot. Indeed, the data from the camera is expressed in its own reference frame $\{C\}$ located at the center of the column, whereas the information provided by the robot is expressed in the reference frame $\{F\}$. The transformation matrix between the robot base frame $\{F\}$ and the reference frame $\{V\}$ of the cluster attached to the vertebra can thus be calculated as follows:

$${}^F\mathbf{T}_V = {}^F\mathbf{T}_R \cdot {}^R\mathbf{T}_V \quad (8)$$

where ${}^F\mathbf{T}_R = \begin{bmatrix} \mathbf{I}_{(3 \times 3)} & {}^F\mathbf{P}_R \\ 0 & 1 \end{bmatrix}$ since we assume that the $\{R\}$ and $\{F\}$ reference frames have perfectly the same orientation. Moreover, ${}^F\mathbf{P}_R$ is obtained following a calibration step which consists in positioning a probe, whose geometry is perfectly known, on the marker corresponding to the origin of the $\{R\}$ cluster. The position of the probe tip is then retrieved thanks to the data sent by the robot and recorded in the vector ${}^F\mathbf{P}_R$. Finally, ${}^R\mathbf{T}_V = ({}^C\mathbf{T}_R)^{-1} \cdot {}^C\mathbf{T}_V$ is determined thanks to the data provided by the motion capture system.

Before performing a drilling, a free manual guidance, or gravity compensation, mode is activated allowing the surgeon to hand-guide the robot until locate the tool at the optimal entry point and along the desired drilling direction. Details of this control mode is provided in section 3.1.1.

Once the tool is positioned according to the desired trajectory, it is possible to switch to a second control mode to allow the robot to follow the movements of the drilling entry point and thus remain aligned to the selected trajectory. The implementation of this mode is explained in section 3.1.2.

In order to allow the robot to follow the movements of the vertebra to be drilled, a new virtual reference frame is then constructed with the same orientation of the tool and translated to the vertebra cluster as shown in Fig. 14. The transformation matrix between these two reference frames is constant, since they belong to the same solid, and allows all the movements of the cluster fixed to the spine model to be reproduced by the tool.

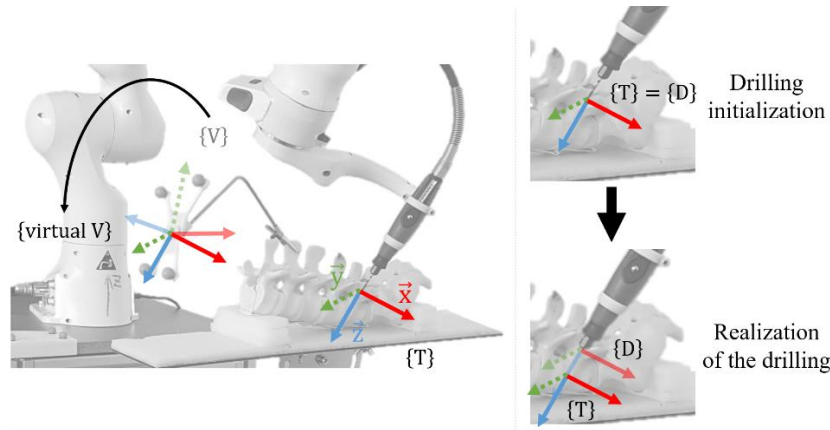


Fig. 14 Representation of the virtual reference frame $\{\text{virtual } V\}$ positioned at the origin of the reference frame $\{V\}$ and according to the same orientation as the tool reference frame $\{T\}$. The reference frame $\{D\}$ is associated with the drilling entry point.

A last transformation matrix is therefore necessary in order to pass from the virtual reference frame to the reference frame $\{D\}$ associated with the drilling entry point initially located at the tool tip. For this purpose, we have considered that the cluster fixed on the spine model and the vertebra to be drilled are part of the same solid. Thus, the transformation matrix, which is then constant, can be defined as:

$${}^{\text{virtual } V}\mathbf{T}_D = \begin{bmatrix} \mathbf{I}_{(3 \times 3)} & {}^{\text{virtual } V}\mathbf{P}_D \\ 0 & 1 \end{bmatrix} \quad (9)$$

where the virtual frame is simply translated at the drilling starting point and ${}^{\text{virtual } V}\mathbf{P}_D$ is obtained knowing the initial position of the tool tip.

Therefore, the drilling entry point can be expressed in the frame of the Franka Emika's base as follows:

$${}^F\mathbf{T}_D = {}^F\mathbf{T}_{\text{virtual } V} \cdot {}^{\text{virtual } V}\mathbf{T}_D \quad (10)$$

The changes recorded in terms of position and orientation of this last matrix have to be sent as instructions to the cobot so that it reproduces the same movements as the vertebra considered and thus maintains the desired drilling trajectory.

REFERENCES

- [1] Paris Spine Institute, Cervical spine, <https://institutdurachis.com/pathologies-rachis/rachis-cervical/>, last accessed 16/03/2021
- [2] Farooq Usmani, M., Gopinath, R., Camacho, J.E., Gentry, R.D., Ludwig, S.C., 2019, "Management of cranio-cervical injuries: C1-C2 posterior cervical fusion and decompression," *Seminars in Spine Surgery*, 32(1). DOI: 10.1016/j.sems.2019.100782
- [3] Huang, M., Tetreault, T.A., Vaishnav, A., York, P.J., Staub, B.N., 2021, "The current state of navigation in robotic spine surgery," *Annals of Translational Medicine*, 9(1). DOI: 10.21037/atm-2020-ioi-07
- [4] Du, W., Zou, D., Zhang, J., Liu, J., Qu, W., Zhang, S., 2021, "Guide wire displacement in robot-assisted spinal pedicle screw implantation," *Videosurgery and Other Miniinvasive Techniques*, 16(3). DOI: 10.5114/wiitm.2021.103952
- [5] Mason, A., Paulsen, R., Babuska, J.M., Rajpal, S., Burneikiene, S., Nelson, E.L., Villavicencio, A., 2013, "The accuracy of pedicle screw placement using intraoperative image guidance systems: A systematic review," *Journal of neurosurgery*, 20(2). DOI: 10.3171/2013.11.SPINE13413
- [6] Gelalis, I.D., Paschos, N., Pakos, E.E., Politis, A., Arnaoutoglou, C., Karageorgos, A., Ploumis, A., Xenakis, T.A., 2011, "Accuracy of pedicle screw placement: a systematic review of prospective in vivo studies comparing free hand, fluoroscopy guidance and navigation techniques," *European Spine Journal*, 21(2), pp. 247-255. DOI: 10.1007/s00586-011-2011-3
- [7] Molligaj, G., Paun, L., Nouri, A., Girod, P.-P., Schaller, K., Tessitore, E., 2020, "The role of robotics in improving surgical outcome in spinal pathologies," *World Neurosurgery* 140. DOI: 10.1016/j.wneu.2020.05.132
- [8] Menger, R.P., Savardekar, A.R., Farokhi, F., Sin, A., 2018, "A cost-effectiveness analysis of the integration of robotic spine technology in spine surgery," *Neurospine*, 15(3). DOI: 10.14245/ns.1836082.041
- [9] Bargar, W.L., Netravali, N.A., 2019, "Total hip arthroplasty technique: TSolution One," *Robotics in Knee and Hip Arthroplasty*. DOI: 10.1007/978-3-030-16593-2_21
- [10] Monogram Orthopedics, Presentation of the Monogram platform, <https://www.monogramorthopedics.com/>, last accessed 24/03/2021

- [11] Intuitive, Da Vinci Surgical Systems, <https://www.intuitive.com/en-us/products-and-services/da-vinci/systems>, last accessed 5/04/2021
- [12] Avrumova, F., Sivaganesan, A., Alluri, R.K., Vaishnav, A., Qureshi, S.A., Lebl, D.R., 2021, "Workflow and efficiency of robotic-assisted navigation in spine surgery," *HSS Journal*, 17(3). DOI: 10.1177/15563316211026658
- [13] Lonjon, N., Chang-Seng, E., Costalat, V., Bonnafoux, B., Vassal, M., Boetto, J., 2016, "Robot-assisted spine surgery: feasibility study through a prospective case-matched analysis," *European Spine Journal*, 25(3). DOI: 10.1007/s00586-015-3758-8
- [14] Khan, A., Meyers, J.E., Siasios, I., Pollina, J., 2019, "Next-generation robotic spine surgery: First report on feasibility, safety, and learning curve," *Operative neurosurgery*, 17(2). DOI: 10.1093/ons/opy280
- [15] Elswick, C.M., Strong, M.J., Joseph, J.R., Saadeh, Y., Oppenlander, M., Park, P., 2020, "Robotic-assisted spinal surgery: Current generation instrumentation and new applications," *Neurosurgery clinics of North America*, 31. DOI: 10.1016/j.nec.2019.08.012
- [16] Johnson & Johnson, VELYS Digital Surgery, <https://www.jnjmedicaldevices.com/en-US/velys>, last accessed 12/04/2021
- [17] Hagag, B., Abovitz, R., Kang, H., Schmitz, B., Conditt, M., 2011, "RIO: Robotic-arm interactive orthopedic system MAKOplasty: User interactive haptic orthopedic robotics," *Surgical Robotics*. DOI: 10.1007/978-1-4419-1126-1_10
- [18] CCHST, Ergonomics of hand tools, <https://www.cchst.ca//oshanswers/ergonomics/handtools/tooldesign.html>, last accessed 03/05/2021
- [19] Siciliano, B., Khatib, O., 2016, *Springer Handbook of Robotics*, 2nd Edition, Chap. 3 and 6. ISBN: 978-3-319-32550-7
- [20] Salah, S., Sandoval Arévalo, J.S., Moncef, G., Laribi, M.A., Zegloul, S., 2020, "Online payload identification of a Franka Emika robot for medical applications," *Advances in Service and Industrial Robotics*. DOI: 10.1007/978-3-030-48989-2_15
- [21] Dietrich, A., Bussmann, K., Petit, F., Kotyczka, P., Ott, C., Lohmann, B., Albu-Schäffer, A., 2015, "Whole-body impedance control of wheeled mobile manipulators: Stability analysis and experiments on the humanoid robot Rollin' Justin," *Autonomous Robots*, 40(3). DOI: 10.1007/s10514-015-9438-z

- [22] Sandoval Arévalo, J.S., Su, H., Vieyres, P., Poisson, G., Ferrigno, G., De Momi, E., 2018, "Collaborative framework for robot-assisted minimally invasive surgery using a 7-DoF anthropomorphic robot," *Robotics and Autonomous Systems*, 106, pp. 95-106. DOI: 10.1016/j.robot.2018.04.001
- [23] Ayoubi, Y., Laribi, M.A., Courreges, F., Zegloul, S., Arsicault, M., 2016, "A complete methodology to design a safety mechanism for prismatic joint implementation," 2016 IEEE/RSJ International Conference on Intelligent Robots and Systems (IROS), pp. 304-309. DOI: 10.1109/IROS.2016.7759071
- [24] Ayoubi, Y., Laribi, M.A., Courreges, F., Zegloul, S., Arsicault, M., 2018, "Complete design methodology of biomimetic safety device for cobots' prismatic joints," *Robotics and Autonomous Systems*, 102, pp 44-53. DOI: 10.1016/j.robot.2018.01.008
- [25] Kochanski, R., Alahmadi, H., O'Toole, J.E., 2019, "Image Guidance in Minimally Invasive Spine Surgery," *Minimally Invasive Spine Surgery*, pp. 83-92. DOI: 10.1007/978-3-030-19007-1_8
- [26] Kleck, C.J., Johnson, C., Akiyama, M., Burger, E.L., Cain, C.J., Patel, V.V., 2018, "One-step Minimally Invasive Pedicle Screw Instrumentation Using O-Arm and Stealth Navigation," *Clinical Spine Surgery*, 31(5), pp. 197-202. DOI: 10.1097/BSD.0000000000000616

Figure Captions List

- Fig. 1 Illustration of pedicle aiming for a lumbar vertebra
- Fig. 2 Comanipulation robots ExcelsiusGPS (a) from Globus Medical and MAKO (b) developed by Stryker
- Fig. 3 Visualization of the different elements of the robotic platform
- Fig. 4 (a) - (b) CAD models of the two configurations of the tool holder prototype and (c) visualization of the hand position on the real tool holder
- Fig. 5 Representation of the damped elastic behavior induced by the stiffness modification in the transverse directions of the motion axis. In the case of very high stiffness the drill is kept along the desired motion axis (a) while low stiffness values produce tolerated deviations of the drill from the desired motion axis (b)
- Fig. 6 Redundancy representation of the Franka Emika cobot. The desired virtual walls of the robot null-space are defined from the values of the limit angles ψ_{min} and ψ_{max} of the robot elbow.
- Fig. 7 Representation of the virtual safety stop in relation to the spine model and the tool position
- Fig. 8 Evolution of the robot stiffness along the longitudinal axis of the tool
- Fig. 9 Evolution of the real and calculated position of the drilling entry point as a function of time and position relative errors considering each directions of displacement

- Fig. 10 Evolution of the position of the tool tip along the x-and-y axis as a function of the longitudinal displacement of the tool and the values of the applied transverse stiffnesses
- Fig. 11 Photo of an experimental drilling trial carried out by an orthopedic surgeon in the spine model in order to validate the first functionalities of the robotic platform
- Fig. 12 Example of results obtained in terms of evolution of the position of the tool tip with respect to the initial tool reference frame $\{T\}$ and evolution of the force exerted on the tool
- Fig. 13 Reference frames definition for each element of the robotic platform
- Fig. 14 Representation of the virtual reference frame $\{virtual V\}$ positioned at the origin of the reference frame $\{V\}$ and according to the same orientation as the tool reference frame $\{T\}$. The reference frame $\{D\}$ is associated with the drilling entry point.

Table Caption List

Table 1 Results of the experimental drilling trials carried out on the spine model